PASJ: Publ. Astron. Soc. Japan **54**, 793–806, 2002 October 25

Spectroscopic Studies of the Solar Corona II. Properties of Green and Red Emission Lines in Open and Closed Coronal Structures

Jagdev SINGH
Indian Institute of Astrophysics, Bangalore 560034, India
jsingh@iiap.ernet.in
Takashi SAKURAI, Kiyoshi ICHIMOTO, and Yoshinori SUEMATSU
National Astronomical Observatory, 2-21-1 Osawa, Mitaka, Tokyo 181-8588
and
Aki TAKEDA*
Kwasan and Hida Observatories, Kyoto University, Sakyo-ku, Kyoto 606-8502

(Received 2002 April 8; accepted 2002 July 8)

Abstract

We obtained profiles of the green (Fe XIV 5303 Å) and red (Fe X 6374 Å) emission lines simultaneously on 1998 July 18–19 for about 4 hours with a cadence of 10 minutes, covering an area of about $200'' \times 500''$ in the solar corona. The line width (FWHM), intensity, and Doppler shift for both lines were computed using Gaussian fits to the observed line profiles. We then studied any systematic differences in these parameters between closed and open field structures, and their time variations. The derived line widths indicate that the FWHM of the red line increases with height above the limb at a rate of 0.5–2.6 mÅ arcsec^{-1} and the green-line width decreases with height at a rate of 1.2–3.4 mÅ arcsec^{-1}. The difference in the time-averaged values of the widths of the green line in open and closed coronal structures at a given height above the limb is small, whereas the width of the red line in open structures is substantially larger than that in the closed loop-like coronal structures.

Key words: line: profiles — Sun: corona — Sun: magnetic fields — techniques: spectroscopic

1. Introduction

Detailed information on the physical characteristics of the solar corona can be obtained from studies of emission-line profiles of forbidden lines in the visible and infrared wavelengths during a total solar eclipse or with a coronagraph. These observations are limited to the limb regions, in contrast to X-ray and UV observations from space of the whole corona (on the disk and above the limb). However, spectroscopic observations from the ground in the visible and infrared wavelengths still have advantages in spatial and wavelength resolutions.

Although the available observing time is only a few minutes, eclipse observations have been extensively used in the past for spectroscopic studies of the solar corona. Slitless evaluations of line profiles using Fabry–Perot interferograms, pioneered by Jarrett and von Klüber (1955, 1961), have been used at subsequent eclipses by Delone and Makarova (1969, 1975), Marshall and Henderson (1973), Liebenberg et al. (1975), Bessey and Liebenberg (1984), Chandrasekhar et al. (1991), and Raju et al. (1993) to investigate the temperature and velocity structure of the solar corona. The Fabry–Perot instrumentation has the advantage of simultaneous registration of interference fringes over most of the corona, from which line profiles can be evaluated, but has the disadvantage of an uncertainty of the contribution from Doppler-shifted elements to the line profile and nonlinear dispersion especially for inner fringes. Livingston and Harvey (1982), Singh et al. (1982), and Singh (1985) have used a multi-slit technique to obtain emission-line profiles during total solar eclipses to study the flow and temperature structure of the solar corona.

The observations with a coronagraph, although their level of scattered light is higher compared to that during total eclipses, are more suited for a detailed investigation of temporal variations in the temperature, density, and velocity of coronal structures over a long duration of time (e.g., for a few hours). In Singh et al. (1999, Paper I), we simultaneously obtained the profiles of the coronal green line ([Fe XIV] 5303 Å, representing typically a plasma of 2×10^6 K) and the red line ([Fe X] 6374 Å, representing a plasma of 1×10^6 K) on a number of days at several coronal regions covering an area of about $200'' \times 500''$. We found that the ratio of the green-to-red line intensities varied between 0.6–9.2 for different coronal structures, which we interpreted as being due to differences in the temperatures of the coronal structures in the range of $(1.2–1.6) \times 10^6$ K. We also found that the width of the red line in the coronal structures increases with height above the limb, while that of the green line in the same coronal regions decreases with height. This behavior of the line widths indicates the existence of spatially unresolved inhomogeneity in the corona, but the physical interpretation is not straightforward. In Paper I we suggested that the mixing of plasma in middle and higher portions of the coronal structures by microturbulence may account for this behavior.

* Presently at the Institute of Space and Astronautical Science, 3-1-1 Yoshinodai, Sagamihara, Kanagawa 229-8510, and at Solar Physics Research Corporation, 4720 Calle Desecada, Tucson, AZ 85718, U.S.A.

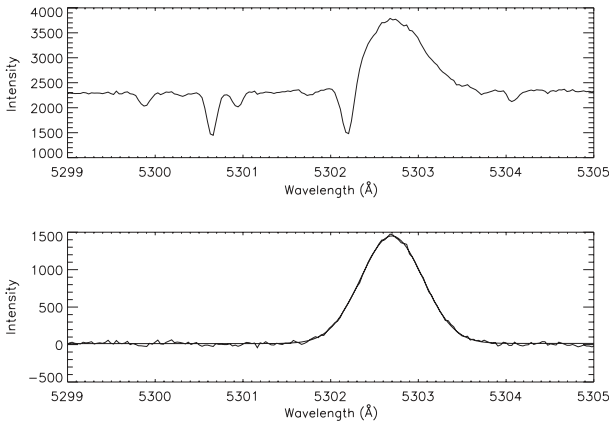

Fig. 1a. The top panel shows a typical observed profile for the green coronal emission line (5303 Å). The bottom panel shows the residual profile after correction for dark current, flat field, and scattered light due to sky brightness along with a Gaussian fit to the residual profile.

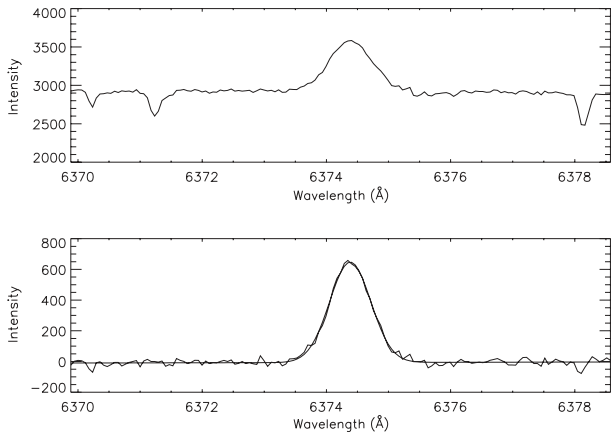

Fig. 1b. Same as (a), but for the red coronal emission line at 6374 Å.

In the present work, we further investigated a data set of Paper I. We selected the data set having the largest spatial coverage and only a slight overlapping of the structures in the field of view. We are primarily interested in gradual changes in the physical and dynamical conditions in coronal structures. We also look into any differences between magnetically closed and open coronal structures.

2. Observations

Spectroscopic observations in two coronal emission lines at 5303 Å and 6374 Å were obtained simultaneously with the 25-cm aperture coronagraph of Norikura Observatory on 1998 July 18–19. The details of the instrumental setup are described in Paper I, and here we only summarize the essential parameter values. A slit width of 200 μm used for observations corresponded to 5″ on the solar image and 77 mÅ and 128 mÅ at the green (fourth order) and the red line (third order) spectra, respectively. Though the spectral resolution was 31.8 mÅ per pixel for the green line and 58.5 mÅ for the red line, the large slit width reduced the overall resolution of the spectra. A raster scan at 50 successive locations in the solar corona was performed in steps of 4″ in the vertical direction (perpendicular to the limb). The exposure time was 10 s for each raster position, and a single raster scan was completed in about 10 minutes. Twenty-six raster scans of the same region were carried out over a duration of more than four hours. The first and the last raster scans were conducted on July 18 2101 UT and July 19 0118 UT. The image scale of the obtained spectra was 2.″25 and 2.″09 per pixel for the red and green lines, respectively.

3. Data Analysis

We followed the method of data analysis developed in Paper I. A Gaussian fit was made to the observed emission-line profile at each location of the observed coronal region to compute its peak intensity, central wavelength, and width of the emission line. These values were then plotted as a function of the spatial locations to produce spectroheliograms, Dopplergrams, and line-width maps of the selected coronal region in the green and red coronal lines.

We computed the Gaussian width (w) from a fit to the observed emission-line profile, which is defined as

$$I(\lambda - \lambda_0) = I(\lambda_0)\exp\left[-\frac{1}{2}\left(\frac{\lambda - \lambda_0}{w}\right)^2\right]. \quad (1)$$

We then obtained the full width at half-maximum (FWHM) of the line, denoted by W, as

$$W = 2(2\ln 2)^{1/2} w = 2.355w. \quad (2)$$

The instrumental line width was corrected as in Paper I. The top panel of figure 1a shows a typical observed line profile for the green coronal emission line. In the bottom panel of the figure we have plotted the residual data after performing a flat-field correction and subtracting the scattered-light component due to the sky brightness. The computed Gaussian fit plotted over the residual data indicates a good fit. Figure 1b shows a typical observed red-line profile, the residual emission-line profile after a flat-field correction and scattered-light subtraction, and a Gaussian fit to the residual data.

Typical errors in fitting the data are listed in table 1 for data points near the limb and at 100″ above the limb. These values indicate very small errors in the computed values of the relative amplitude, wavelength, and FWHM from the Gaussian fit. Most of the time a single Gaussian fit to the observed emission-line profile was found to be satisfactory; at no instance did the observed line profiles show double peaks.

Figure 2a shows heliograms of a coronal region observed at 2111 UT on 1998 July 18. The left and right panels in the top row show the distributions of the red and green line intensities. The middle panels show the line-of-sight velocities, and the lower panels indicate the line-width distribution of the coronal region. The intensity distribution in the red line shows a closed loop-like coronal structure (A + B + C) having some fine structures, and three jet-like structures (D, E, and F). In the green line the coronal region appears to be diffuse with a few fine structures of enhanced intensity. An open structure (G), which

Table 1. Typical errors in the computed relative intensity, FWHM, and central wavelength from the Gaussian fit.

	Near limb	At 100″ above the limb
Green line (5303 Å):		
Relative intensity	±0.021%	±0.11%
FWHM	±0.001 Å	±0.002 Å
Wavelength	±0.001 Å	±0.001 Å
Red line (6374 Å):		
Relative intensity	±0.057%	±0.37%
FWHM	±0.001 Å	±0.003 Å
Wavelength	±0.001 Å	±0.001 Å

is broad and small in height in the vicinity of structure B, was also considered for a detailed analysis. A fine structure (H) that is only seen in the green-line image lies just at one edge of the loop-like structure A marked in the red-line image. Figure 2b indicates these structures in a sketch of the coronal structures.

In figure 3 we show the development of the coronal region in the red and green lines with time. The time of observation is indicated at the top of each image.

The procedure adopted to determine the relation between the parameters of the two lines is basically the same as in Paper I. Namely, the pixel corresponding to a spatial dimension of $4'' \times 4''$ was marked with the help of a cursor in the red-line image displayed on the monitor, and the corresponding location in the green-line image was identified by a computer program. The parameters of the green and red emission lines were then determined from the respective intensities, velocities, and widths maps.

In Paper I, we only produced correlation plots among line intensities and FWHM, and the line intensities were used as an indicator for the heights in the corona (lower heights corresponding to larger intensities, and vice versa). In the present study, the line parameters were plotted as a function of height above the limb. It will be more appropriate to plot the parameters as a function of the actual distance along the structure. However, this needs information or an assumption on the geometrical shape of the structure.

To begin with, all of the coronal structures visible in the observed region were considered together and the line widths, relative intensities, and velocities were computed to see the general trend in these parameters. We have selected 200 locations with a resolution of $4'' \times 4''$ on various coronal structures visible in the red-line images, shown by the dark squares in figure 4. The corresponding locations in other images were selected automatically by software. These pairs of images appear to be similar, even though the fine structures do not overlap exactly with each other. The differences in the images may be due to different temperatures and densities in different parts of this broad coronal structure.

Similarly, we performed an analysis for individual open and closed coronal structures by selecting 15–20 locations depending upon the length of the individual structure, in order to investigate the physical differences between these two kinds of structures. We sub-divided the broad closed loop-like structure seen in the red-line image into three parts: two vertical parts (A and B) and a horizontal part (C). The two vertical parts were further divided into four sub-structures whose centers are shown in figure 2b by black lines: two at the edges of the structure and two in between the edges. Due to the large area occupied by the top of the loop-like structure (C), 50 pixels were allocated to derive the values of line parameters. The broad jet-like structure F was divided into two sub-structures. In total, we have 14 structures and sub-structures.

4. Results

4.1. Spatial Variation in Line Parameters: All Structures Included

The top panel of figure 5 shows a scatter plot of the green-line intensity (I_g) versus the red-line intensity (I_r). The middle panel shows a plot of the green-line widths (W_g) in triangles and the red-line widths (W_r) in asterisks, as a function of height h above the limb. The bottom panel shows a plot of the intensity ratio (I_g/I_r) against height in arcsecond. These plots were made from the data of July 19 0108 UT.

The top panel shows a loose correlation between I_g and I_r. The scatter is due to the mixture of structures with various values of temperatures and densities. Later we will see that a good correlation is obtained if we isolate a single structure.

The middle panel indicates that W_g decreases with height, while W_r increases with height above the limb, confirming the earlier results of Paper I. The linear fits are also indicated in the middle panel. The gradients in this case are $dW_g/dh = -1.57\,\mathrm{m\AA\,arcsec^{-1}}$ and $dW_r/dh = 0.51\,\mathrm{m\AA\,arcsec^{-1}}$, respectively.

The bottom panel shows that the intensity ratio (I_g/I_r) lies between 2–10 near the limb and between 1–3 at 150″ above the limb. It is also noticed that the spread in the I_g/I_r values becomes smaller (i.e., inhomogeneity becomes smaller) at larger heights. Raju and Singh (1987) computed the expected intensities of the green and red lines as a function of the temperature and radial distance from the solar surface. A spherical symmetry was assumed to compute the line intensities integrated along the line of sight. The radial distance in their analysis specifies both the density (through a certain model) and the geometrical dilution factor of radiation. For the low corona being studied in the present analysis, the effect of dilution factor is small. We could therefore translate their results, and have evaluated the line intensities as a function of temperature and density. Table 2 gives the expected line-intensity ratio, I_g/I_r, as a function of temperature. The range in the intensity ratio corresponds to a density range of $(0.4\text{–}1.5) \times 10^8\,\mathrm{cm^{-3}}$. A representative temperature corresponding to the observed ratio I_g/I_r of about 5 is 1.5×10^6 K. A tendency of decreasing temperature as a function of height can be seen in the bottom panel of figure 5.

4.2. Spatial Variation in Line Parameters: Individual Structures

Figures 6a–e show analyses similar to figure 5, carried out for individual structures: the edge of structure A (figure 6a), the inner part of structure A (figure 6b), the top part of loop C (figure 6c), an open structure D (figure 6d), and the broad

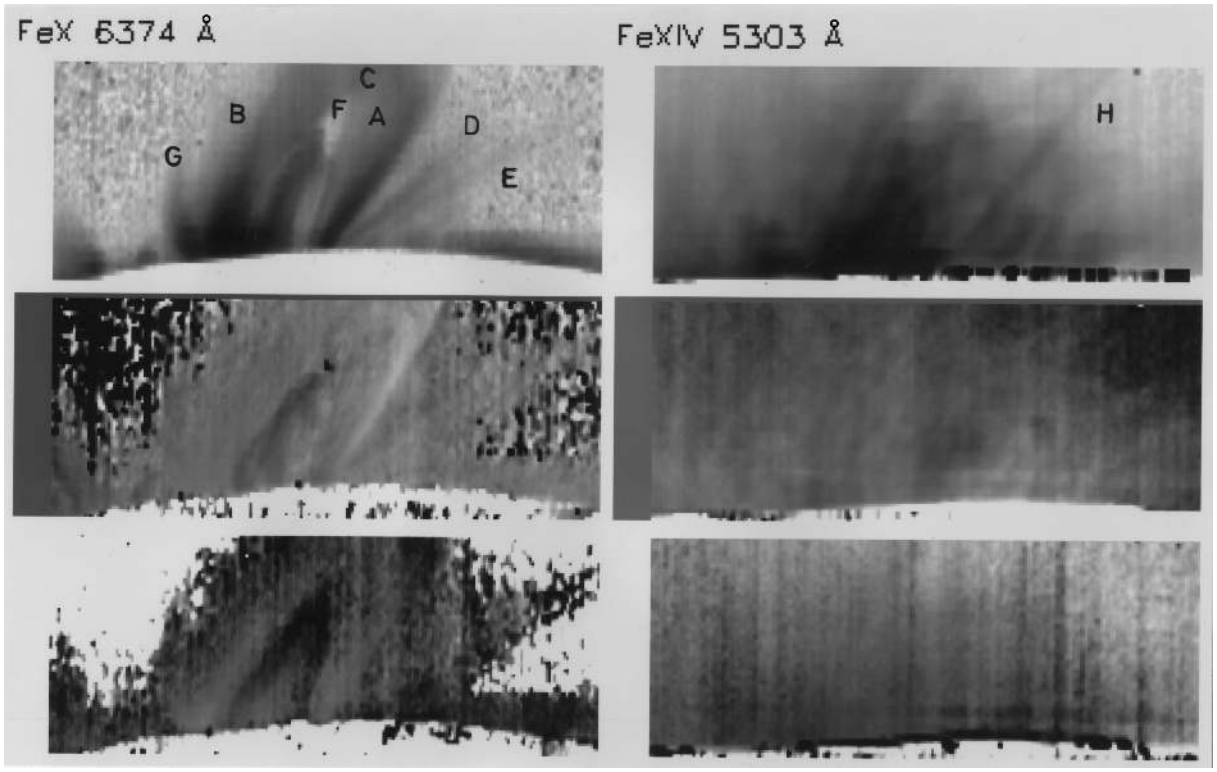

Fig. 2a. Images of the solar corona constructed from the line profiles observed on 1998 July 18. The top row shows the distribution of the red and green line intensities in the observed coronal region. The middle and bottom rows indicate the velocity and line-width distributions, respectively. The range of velocities shown in the gray scale is from -7.0 to $+6.8\,\mathrm{km\,s^{-1}}$ for 6374 Å and from -6.2 to $+4.5\,\mathrm{km\,s^{-1}}$ for 5303 Å. The line widths in the range of 0–1.5 Å are represented in gray scale.

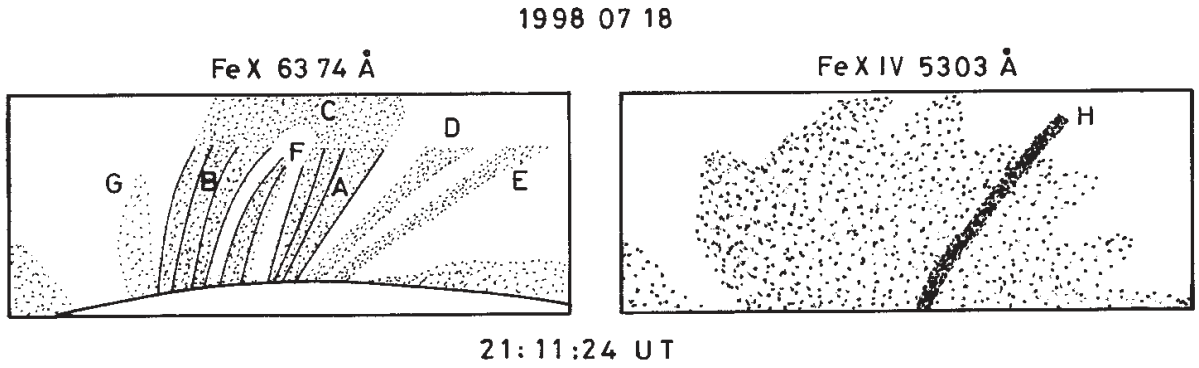

Fig. 2b. Sketch of prominent coronal structures made by tiny dots. The black lines indicate some of the sub-structures studied in a detailed analysis. Structure 'H' in the green-line image lies just at the edge of structure 'A' in the red-line image.

jet-like structure F (figure 6e). These plots were made from the data of July 19 0108 UT.

In each figure, the scatter plot (top panel) between the green-line intensity (I_g) and the red-line intensity (I_r) now shows a tight correlation. This indicates that the variations in I_g and I_r along each structure are mostly due to density inhomogeneity that is eventually cancelled out when taking the ratios. Therefore, the least-square regression line is also shown in each panel. The slope of linear fit ($\delta I_g/\delta I_r$) varies between 1 to 10.

The middle panels in figures 6a–e indicate that, in all cases, the green-line width W_g decreases with height above the limb, while the red-line width W_r increases with height. A possible exception may be in figure 6c (structure C at the top of the loop), where the variations of line widths with height are insignificant.

In the bottom panels of figures 6a–e, we see that the ratio I_g/I_r, which lies between 0.5 to 14, varies with height, meaning that there is residual inhomogeneity in temperature or density. This ratio is different for different structures; for some structures the ratio increases with height and for some others it decreases with height above the limb; and for some structures the ratio increases up to some height and then decreases.

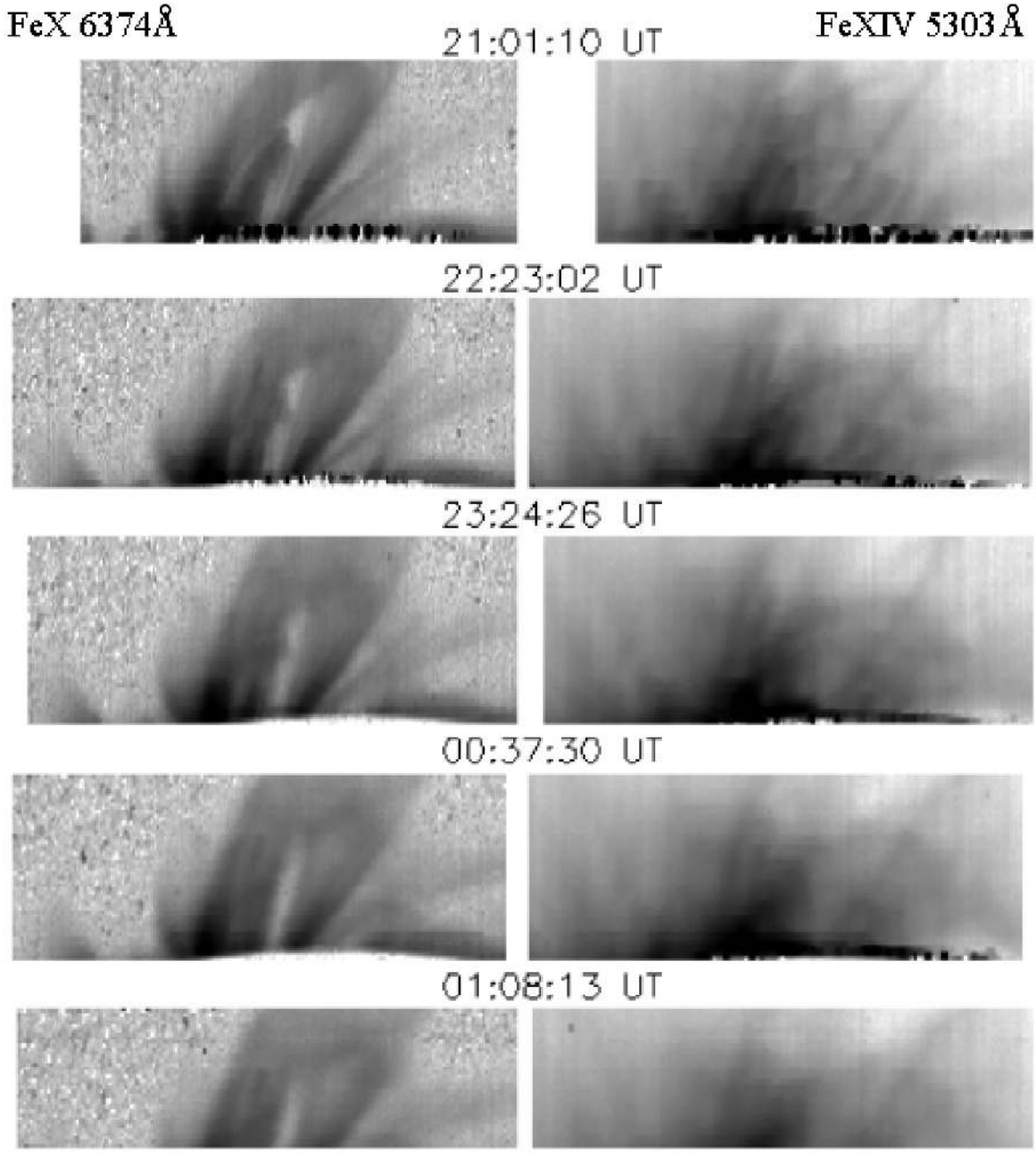

Fig. 3. Images of the coronal region in the red and green emission lines as a function of time, showing development of the coronal structures. The epoch of observation is indicated above each image.

Figure 6c is exceptional here as well, and shows a large scatter in the correlation plot between I_g and I_r and in the height variations of the ratio of I_g/I_r. This may be due to overlap of several structures along the line of sight.

If the ratio I_g/I_r is constant in height, it means that the temperature is constant in height. We thus expect that the correlation plot, I_g versus I_r, shows a linear relationship with zero y-intercept. The fitted line often shows a positive y-intercept (figures 6a and e), meaning that the green-line emission dominates at larger heights (at smaller emission-line intensities). This can be rephrased that the temperature increases with height. In such a case, the interpretation of the slope of linear fit ($\delta I_g/\delta I_r$) is not straightforward; it may represent a combination of the temperature and its gradient in height. It is interesting that generally the scatter plot between I_g and I_r shows a tighter, linear relationship, even when the ratio I_g/I_r does not show a systematic behavior as a function of height.

4.3. Time Variations in Coronal Structures

The top left-hand-side image in figure 3 shows the intensity distribution in the red emission line at the beginning of observations. The subsequent images in the red and green emission

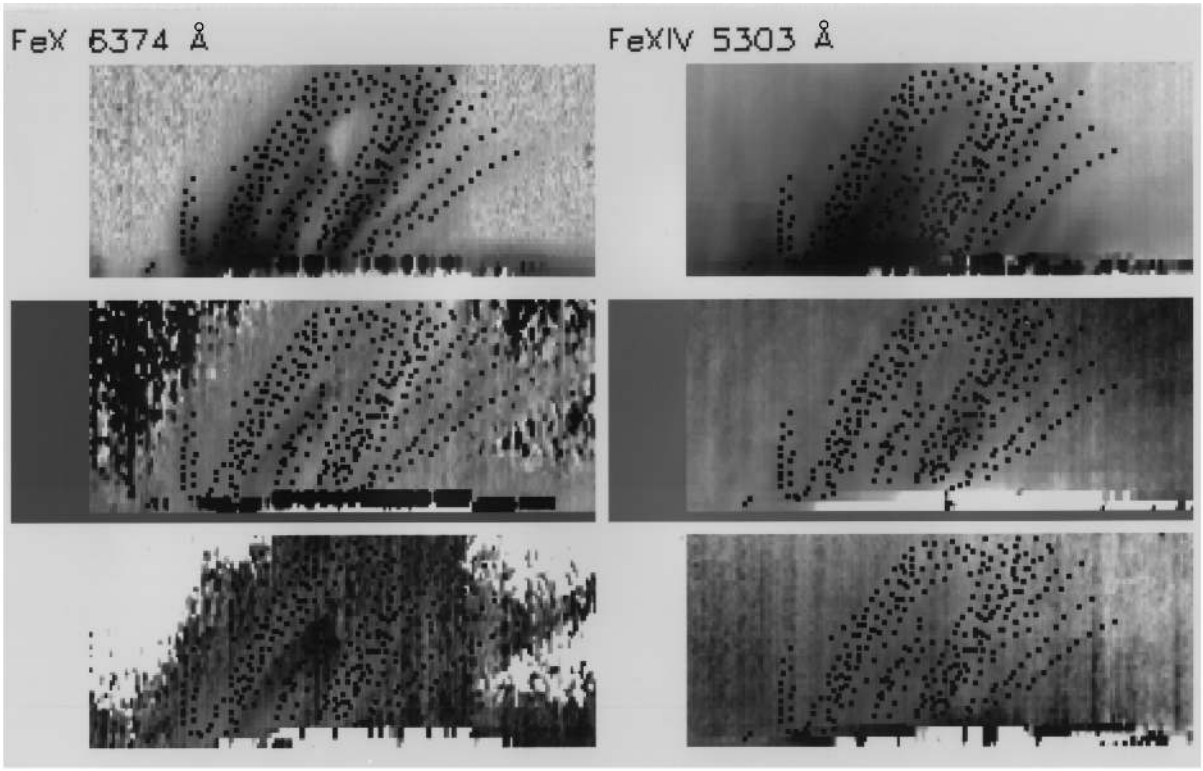

Fig. 4. Same as figure 2a. The small black squares show the locations on the coronal structures where the values of the line width, intensity, and velocity have been determined to generate figure 5.

lines, obtained for about four hours, show the growth of coronal structures in this region. It is clear that the general shape of the coronal structures remained more or less the same. However, the width of both the vertical portions of the loop-like coronal structures increased by about 10% during the observations. Such a change is unlikely to be due to the rotation of the Sun and the projection effect. On the contrary, the intense jet-like structure F showed faster changes in intensity and appeared to become longer in size.

To study the time variations in these structures, we computed the values of FWHM at 50″ and 100″ above the limb [denoted by $W(50'')$ and $W(100'')$] for all of the structures as a function of time. We also determined the slopes of a linear fit, $\delta I_g/\delta I_r$, for all of the above-mentioned 14 structures as a function of time. The left-hand-side panel of figure 7a indicates the variations of $W_g(50'')$ (solid), $W_r(50'')$ (dashed), $W_g(100'')$ (dotted), and $W_r(100'')$ (dash-dotted), respectively, as a function of time on the edge of the vertical coronal structure A. The right-hand-side panel of figure 7a depicts the variations in dW_g/dh (solid), dW_r/dh (dash-dotted), and $\delta I_g/\delta I_r$ (dotted) with time. Figure 7b indicates the variations in these parameters for the middle portion of the vertical structure A. Figures 7c–e show the variations in the top of loop C, the open jet-like structure D, and the broad intense jet-like structure F, respectively. In table 3 we list the time-averaged values of these parameters for all 14 structures.

The plots of $W(50'')$, $W(100'')$, and dW/dh as a function of time (figures 7a–e) indicate that both $W_g(50'')$ and $W_r(50'')$ increased slowly with small fluctuations for about three hours, and then started decreasing in most of the individual structures. The width $W_r(100'')$ showed a similar trend, whereas $W_g(100'')$ showed some random variations with no systematic increase or decrease with time. On the average, both $W_g(50'')$ and $W_r(50'')$ increased by about 4% over a period of four hours, whereas at 100″ only the red-line width $W_r(100'')$ increased by about 9% in this interval.

In structures D and F (figures 7d and e), $W(100'')$ fluctuated more than $W(50'')$. Spiky time variations in $W(50'')$ and $W(100'')$ were generally correlated for the red-line data and for the green-line data individually. However, W_g and W_r sometimes showed anti-correlation.

The slope $\delta I_g/\delta I_r$ for all 14 structures indicate an increase in the values with time. This implies an increase in temperature in this active region as a whole.

The gradients dW_g/dh and dW_r/dh both fluctuated around the mean value during the entire span of four hours. The gradient of the line width in different sub-structures showed different trends as a function of time. For the green line, the gradients stay constant in figures 7a and b, but attain more negative values in figures 7c–e. For the red line, the gradients increase in figures 7b and d, and decrease in figure 7e. We may interpret that the gradient of the line width represents the concentration of non-thermal energy input; a large and positive (negative) gradient indicates a preferentially larger non-thermal width in the top (footpoint) part of the structure, respectively. The complex behavior of the gradients of the line width implies that the non-thermal energy input is not stationary and changes its preferential location of deposition along the structure.

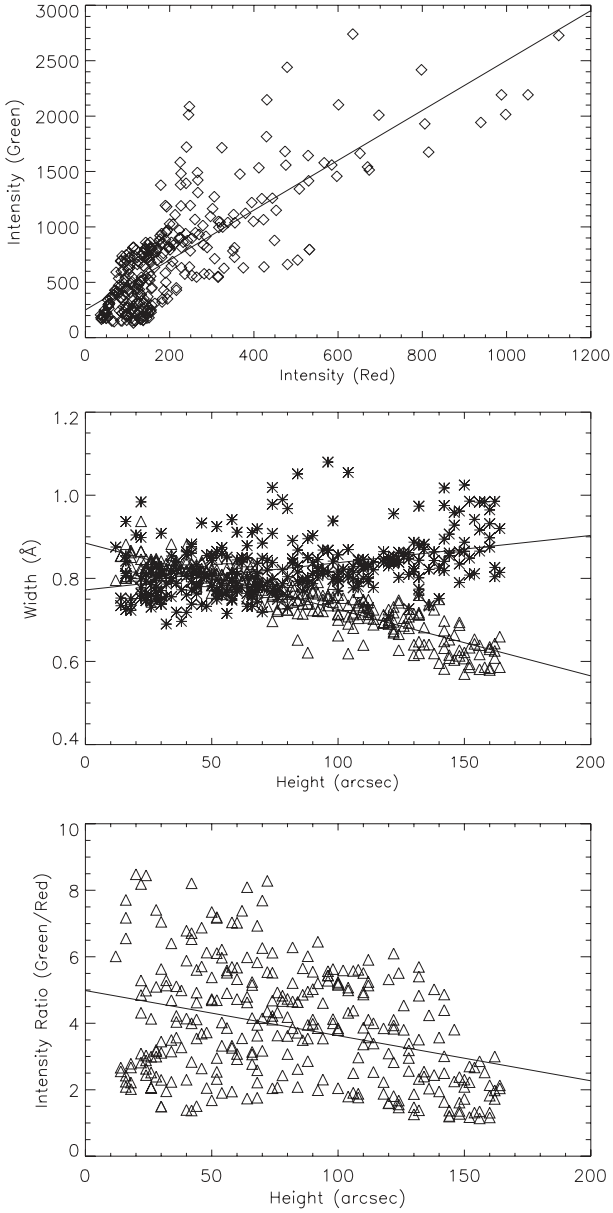

Fig. 5. Typical plot made after computing the values of line width, intensity, and velocity over a $4'' \times 4''$ coronal region by considering all the structures together. The top panel shows the variation of the green-line intensity versus the red-line intensity for structures observed on 1998 July 19 at 0108 UT. The middle panel represents the FWHM of the green (△) and red (∗) line as a function height above the limb along with linear fits (straight lines) to the respective data. The bottom panel shows the intensity ratio (I_g/I_r) versus height above the solar limb.

4.4. *Intensity Ratio and Temperature*

In general, the intensity ratio of the green to red lines (I_g/I_r) is different for different coronal structures and sub-structures. The values of I_g/I_r observed between 0.5 and 14 imply a temperature range of $(1.2–1.7) \times 10^6$ K (table 2).

The intensity ratio I_g/I_r is generally greater near the edges of a coronal structure than in the inner part of the structure, as is seen in the snapshot plots (figures 6a and b). The time-averaged values listed in table 3 also indicate larger values for the slope $\delta I_g/\delta I_r$ at the edges of coronal structures A and B in comparison with the inner portion of the same structures. Also, the time-averaged values of W_r are larger for the edges of structures A and B, as compared to the inner portion of the structures (table 3). Large values of $\delta I_g/\delta I_r$ and higher values of W_r at the edges of the coronal structures imply a higher temperature and/or non-thermal velocity at the edges (sheath) in comparison with the inner portion (core) of the coronal structures.

Table 2. Ratios of the green-line intensity I_g and the red-line intensity I_r as a function of temperature (taken from Raju, Singh 1987).

Temperature ($\times 10^6$ K)	I_g/I_r
1.1	0.24–0.48
1.2	0.54–0.86
1.3	1.2–1.5
1.4	2.1–2.7
1.5	4.2–5.3
1.6	8.3–9.5
1.7	15–18
1.8	26–39

4.5. *Line-Width Variation with Height*

In all of the 14 structures studied, W_g decreased and W_r increased monotonically with height above the limb. The time-averaged values of $W_g(50'')$ and $W_g(100'')$ for different structures show a small range, whereas those for $W_r(50'')$ and $W_r(100'')$ show a large range (table 3). The mean values for the red line are greater for open structures and edges of the structures, as compared to the closed structures and the inner portions of the coronal structures, respectively. Consistently with this result, Raju et al. (2000) found that the line widths in closed magnetic structures are smaller than those in open field structures in the polar regions.

By temporal averaging over each structure, and then over all of 14 structures, we obtained the average FWHM of the green and red lines as $\overline{W_g(50'')} = 0.813$ Å and $\overline{W_r(50'')} = 0.816$ Å, respectively, at $50''$ above the limb. Assuming that the line widths are entirely due to thermal broadening, the temperature corresponding to these values are 2.56×10^6 K and 1.78×10^6 K, respectively. These values are much higher than the ionization temperatures, 1.8×10^6 and 1.0×10^6 K of [Fe XIII] and [Fe IX] ions, respectively. We find that the average intensity ratio of the green to red lines is about 5, which corresponds to a temperature of 1.5×10^6 K. Assuming this value for the temperature of these coronal structures, from the above-mentioned values of FWHM, we derived the values of non-thermal component of velocity V_t using

$$\frac{2kT}{M} + V_t^2 = \frac{1}{4\ln 2} c^2 \frac{W^2}{\lambda^2}, \quad (3)$$

where T is the coronal temperature, M is the mass of the ion, c is the velocity of light, W is the FWHM of the line profile, and λ is the wavelength of the coronal emission line. The thus-obtained values for non-thermal velocities are 17.8 km s^{-1} and

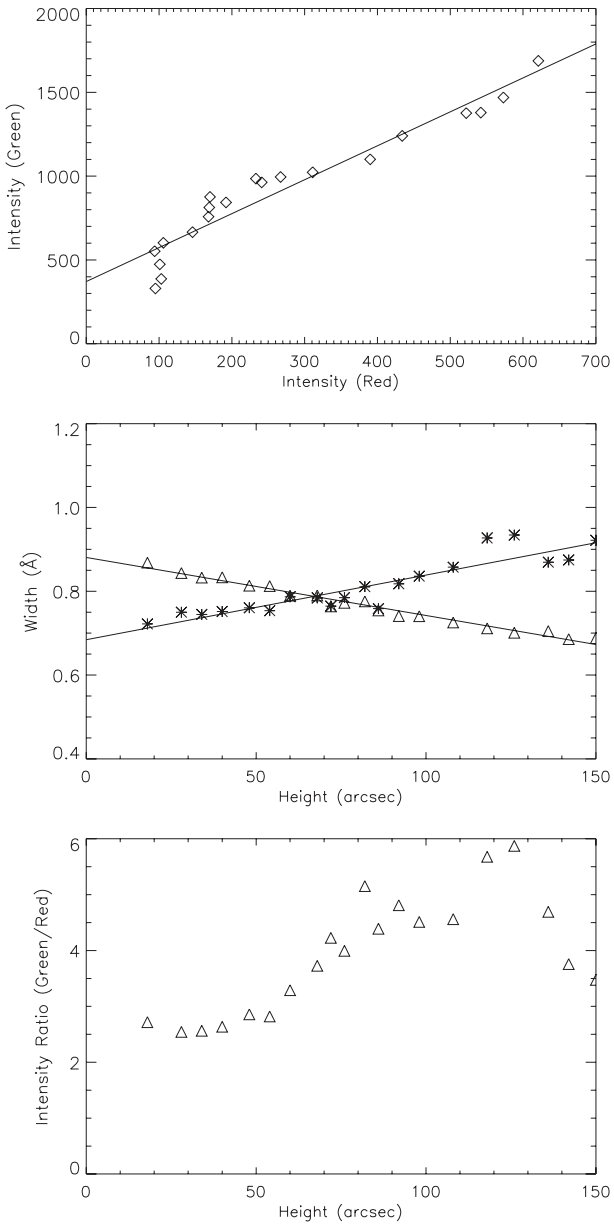

Fig. 6a. Same as figure 5, but for an individual structure; the edge of the closed loop-like structure (A).

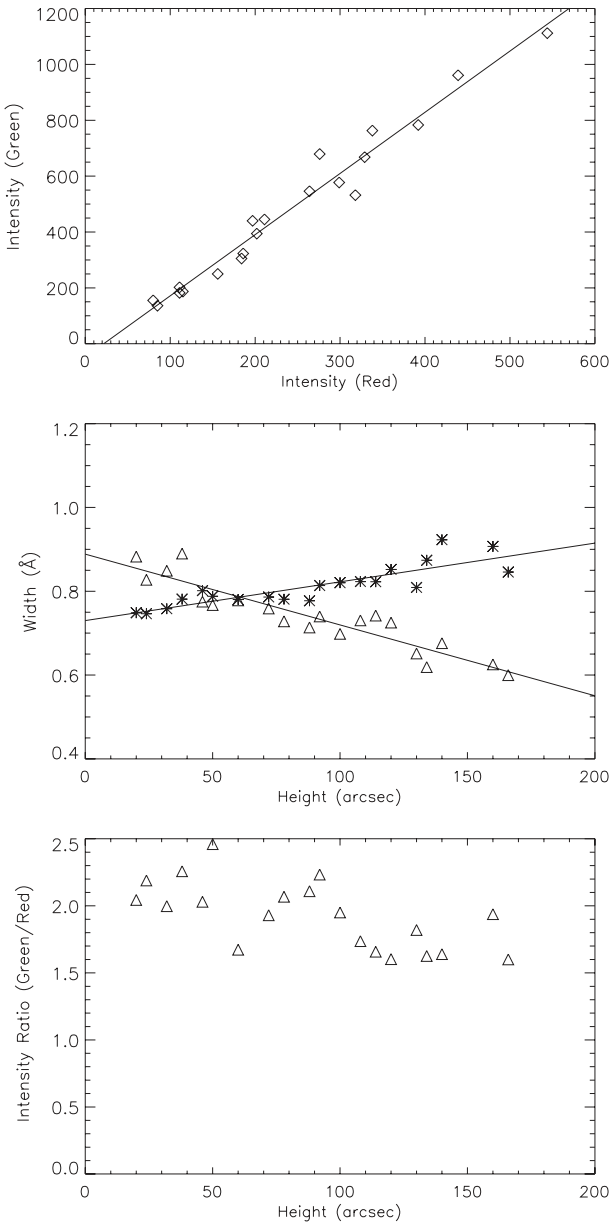

Fig. 6b. Same as figure 6a, but at a different epoch and for an individual structure inside the loop-like structure A.

$9.2\,\mathrm{km\,s^{-1}}$ for the green and red lines, respectively.

The large difference in the derived non-thermal velocities indicates that the plasmas emitting the green line and the red line are different. We may thus assign different values of temperature to these plasma components. If the green line comes from a plasma (hot component) of $1.8 \times 10^6\,\mathrm{K}$ and the red line comes from a plasma (cool component) of $1.0 \times 10^6\,\mathrm{K}$, the non-thermal velocities are $15.0\,\mathrm{km\,s^{-1}}$ and $15.3\,\mathrm{km\,s^{-1}}$ for the green and red lines, respectively. However, this is a rather extreme case. If the hot component is $1.6 \times 10^6\,\mathrm{K}$ and the cool component is $1.3 \times 10^6\,\mathrm{K}$, for example, the green line still primarily comes from the hot component and the red line primarily comes from the cool component, and the non-thermal velocities are $16.9\,\mathrm{km\,s^{-1}}$ and $12.0\,\mathrm{km\,s^{-1}}$ for the green and red lines, respectively.

At a height of $100''$, the time-averaged values of FWHM over all structures are $\overline{W_\mathrm{g}(100'')} = 0.727$ Å and $\overline{W_\mathrm{r}(100'')} = 0.882$ Å for the green and red lines, respectively. Assuming $T = 1.5 \times 10^6\,\mathrm{K}$, we find non-thermal velocities of $12.8\,\mathrm{km\,s^{-1}}$ and $13.2\,\mathrm{km\,s^{-1}}$ for the green and red lines, respectively. These two values are close to each other, indicating an identical volume of plasma as the source of emission at a height of $100''$. In contrast, at a height of $50''$ the non-thermal velocities are larger for the green line and are smaller for the red line compared to the values at $100''$. The temperatures of the hot (cool) component at $50''$ are lower (higher) than the corresponding values at $100''$, but the differences are small.

The top part of the loop-like structure C extended from about

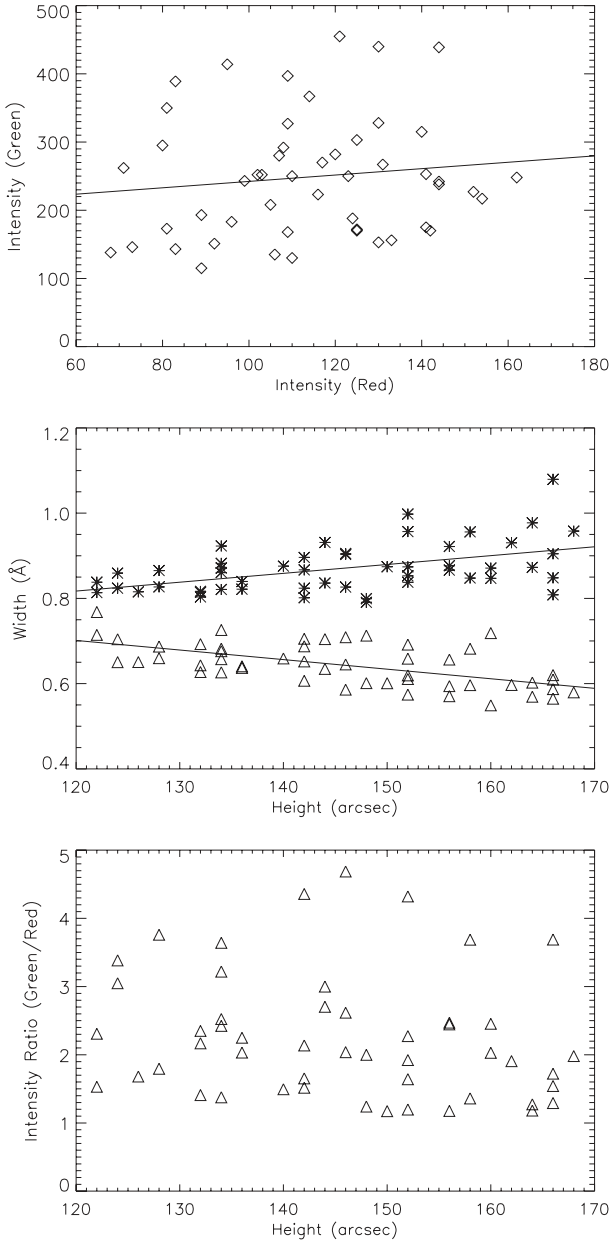

Fig. 6c. Same as figure 6a, but for the top portion marked C of the loop-like structure.

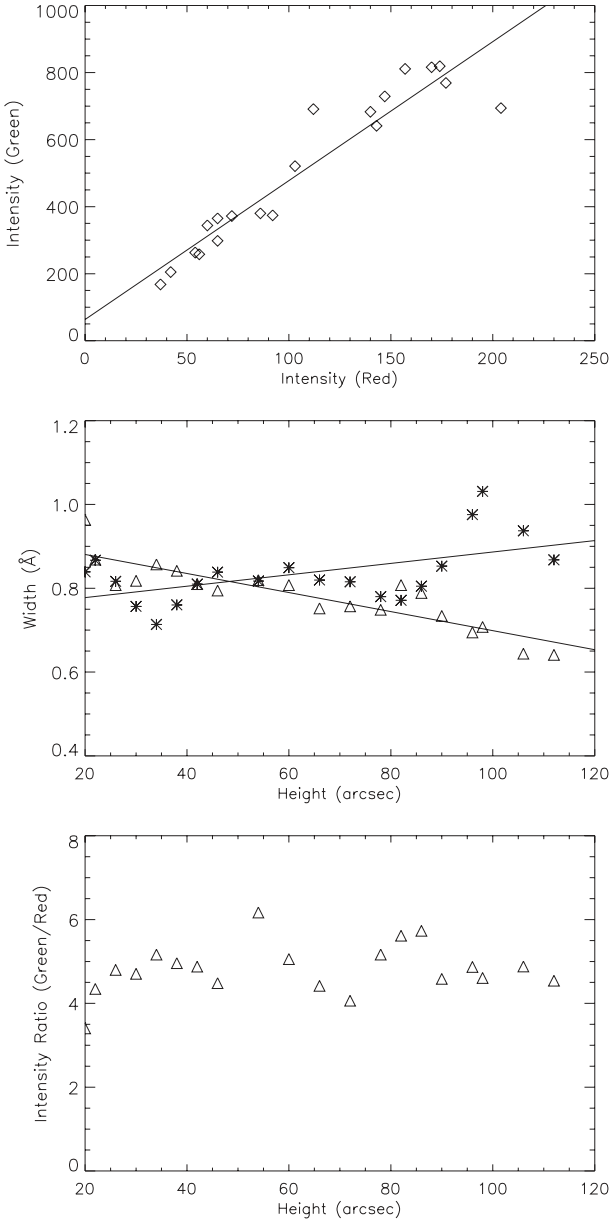

Fig. 6d. Same as figure 6a, but for the jet-like structure D.

120″ to 170″ above the limb and appeared to join the vertical structures A and B seen in the red-line coronal images. The time-averaged values of FWHM at 150″ for the green and red lines are $\overline{W_g(150'')} = 0.636 \pm 0.023$ Å and $\overline{W_r(150'')} = 0.882 \pm 0.018$ Å, respectively. The green-line width corresponds to a temperature of 1.57×10^6 K, while the red-line width corresponds to 2.08×10^6 K if we assume that the observed line width is completely due to thermal broadening. The temperature corresponding to the width of the green line is less than the ionization temperature of [Fe XIII], whereas that corresponding to the red-line width is much greater than the ionization temperature of [Fe IX]. The intensity ratio I_g/I_r, which is about 2, changed by a very small amount during the interval of observations. Table 2 indicates that the ratio (I_g/I_r) of 2 corresponds to a temperature of 1.4×10^6 K. Assuming this to be the real temperature of the top part of the coronal structure, we find that the green-line width of 0.636 Å yields a micro-turbulent velocity of 7.0 km s^{-1} and the red-line width of 0.882 Å yields a turbulent velocity of 14.3 km s^{-1}. The difference in the derived values of non-thermal velocities for the green and red lines may be partly due to a difference in the assumed and real temperatures of the structure.

4.6. Gradient of the Green and Red Line Widths

The time-averaged values of the width gradients are steeper in open coronal structures as compared to those in close structures, implying larger changes in temperature or non-thermal velocity with height in open structures than in closed structures. The scatter plot of time-averaged values of FWHM gradient

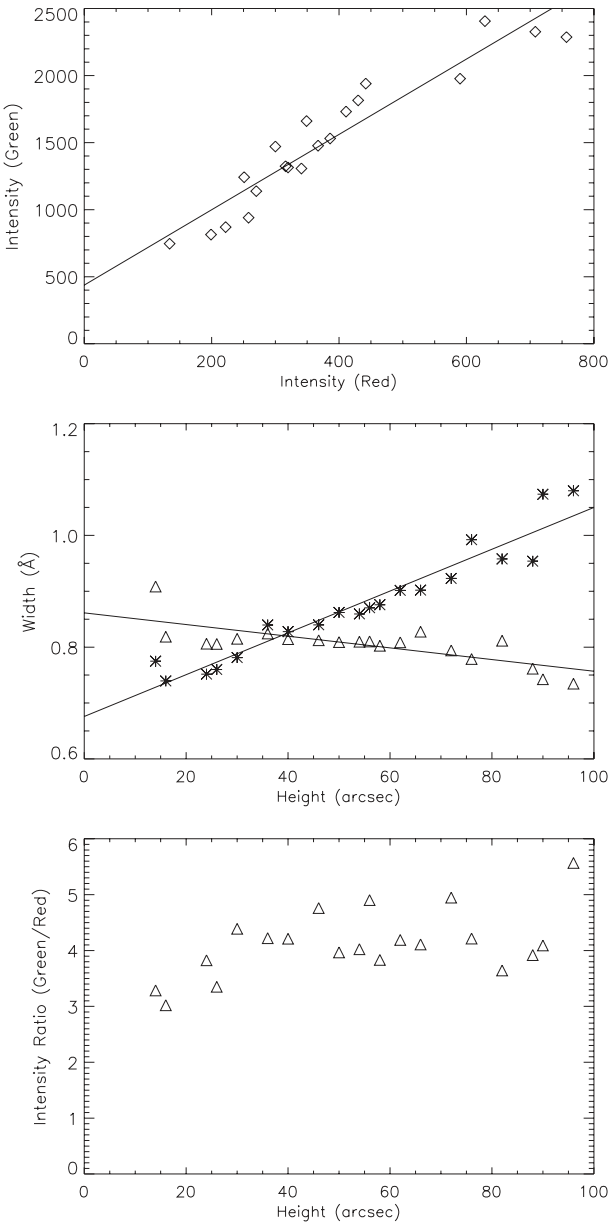

Fig. 6e. Same as figure 6a, but for the broad intense jet-like structure F.

$-dW_g/dh$ versus dW_r/dh shown in figure 8 indicates a loose, but negative, correlation between these two. Namely, when dW_g/dh is steeper (more negative), then dW_r/dh is positive and smaller, and vice versa. This negative correlation may imply that the gradients of line width depend upon the temperature of the structure: the higher is the temperature, the steeper (more negative) is the gradient of the width of the green line, and the less steeper (positive but smaller) is that of the red line. This tendency fits into a more general property that the hotter green line generally shows a negative gradient of the width and the cooler red line shows a positive gradient of the width, and leads to a guess that intermediate ions [Fe XI]–[Fe XIII] may show a gradient that is between the green and red line values. More data are needed to establish the relationship between the gradients of various ions quantitatively. An analysis of observations made for both [Fe X] and [Fe XI] lines simultaneously is under way.

4.7. Line-Widths in Open and Closed Structures

We have compared a closed loop-like structure (A+B+C) and five open coronal structures including two sub-structures. The mean values of FWHM for the green line are $W_g(50'', \text{closed}) = 816 \pm 2$ mÅ and $W_g(100'', \text{closed}) = 731 \pm 10$ mÅ, respectively, for the closed coronal structure; while they are $W_g(50'', \text{open}) = 810 \pm 10$ mÅ and $W_g(100'', \text{open}) = 726 \pm 19$ mÅ for the open structures, respectively. The corresponding values for the red line are $W_r(50'', \text{closed}) = 794 \pm 18$ mÅ and $W_r(100'', \text{closed}) = 852 \pm 16$ mÅ for the closed structure, and $W_r(50'', \text{open}) = 851 \pm 20$ mÅ and $W_r(100'', \text{open}) = 940 \pm 51$ mÅ for the open structure, respectively. These and the values listed in table 3 for the individual coronal structures indicate that the width of the green line is almost the same in the closed and open coronal structures, whereas the width of the red line is significantly greater in open coronal structures as compared to that in closed structures. The difference in the widths of the red line for open and closed structures is greater at larger heights in comparison with that at smaller heights. It is surprising to note that only the red line shows larger values of the width in open structures as compared to closed structures.

The mean values of the gradient of the FWHM of the green and red lines are $\overline{dW_g/dh} = -1.7 \pm 0.2$ mÅ arcsec^{-1} and $\overline{dW_r/dh} = 1.1 \pm 0.6$ mÅ arcsec^{-1}, indicating that the spread is large in the case of the red line. The broad intense structure F shows a steeper gradient for the red line and less-steep gradient for the green line as compared to those of the closed structures. In contrast, other three open structures indicate steeper gradient for the green line and flatter gradient for the red line. More data are needed to understand why such a kind of behavior exists in open coronal structures.

4.8. Effect of Mass Motions inside the Coronal Loops

There exists a velocity pattern in coronal structures in our data, but the magnitude of velocities is small. Raju (1999) has discussed the effects of large-scale velocities on the broadening of coronal emission lines, and has reported the existence of multi-components in coronal emission-line profiles. In the present observations we found that almost all the observed line profiles could be fitted with single Gaussian curves, and most of the locations along the coronal structures showed normal values of widths for both the green and red lines. Therefore, our conclusions on the line-width variations are not affected by large-scale mass motions.

5. Discussion

We cannot explain the observed increase in the width of the red line and the decrease in the width of the green line with height, if the two lines are emitted from the same volume of plasma. The interpretation requires the introduction of some kind of inhomogeneity. In Paper I we suggested the following. The coronal structures, although they are broadly guided by magnetic fields, may have internal structures in temperature and density. At the bottom of the coronal structures where the

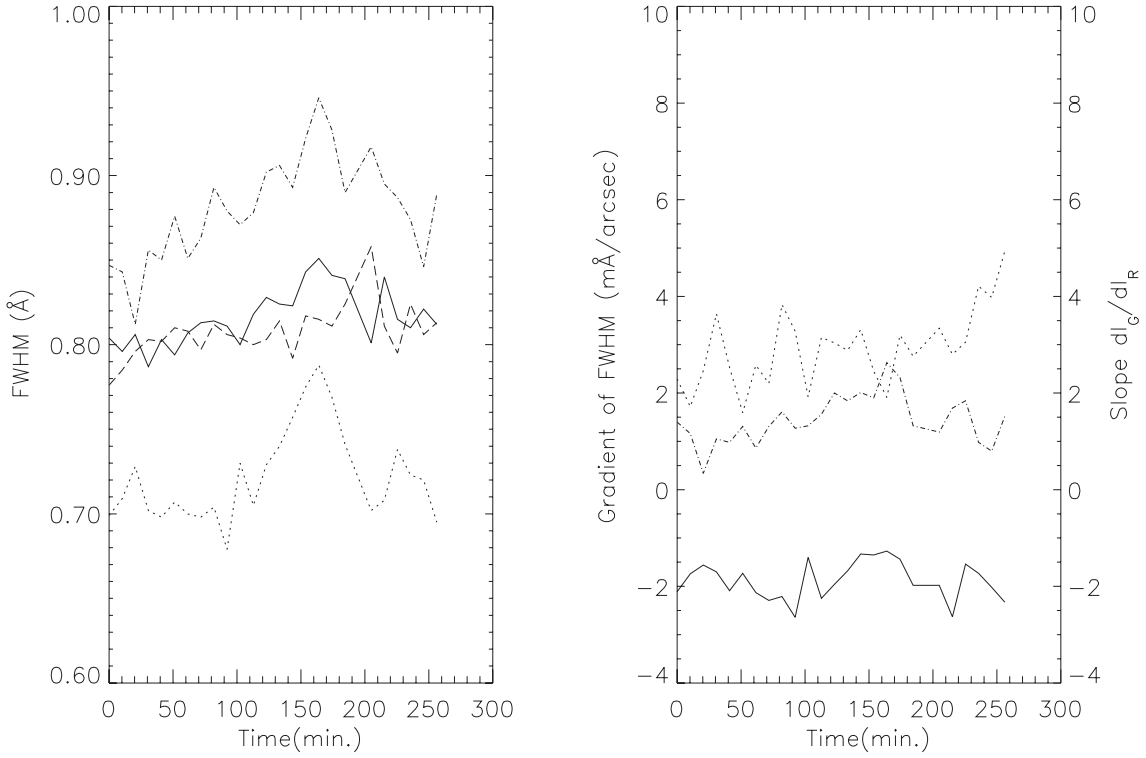

Fig. 7a. Typical plots of W (FWHM) at $50''$ and $100''$ and gradients dW/dh of the green and red lines as functions of time for one of the edges of the vertical part A of the loop-like structure in figure 2b. In the left-hand-side panel of the figure, the solid and dashed curves indicate $W_g(50'')$ and $W_r(50'')$, respectively, and the dotted and dash-dotted curves show $W_g(100'')$ and $W_r(100'')$, respectively. In the right-hand-side panel, the solid and dash-dotted curves represent dW_g/dh and dW_r/dh, respectively, and the dotted curve shows the variation of the slope of the linear fit $\delta I_g/\delta I_r$ with time.

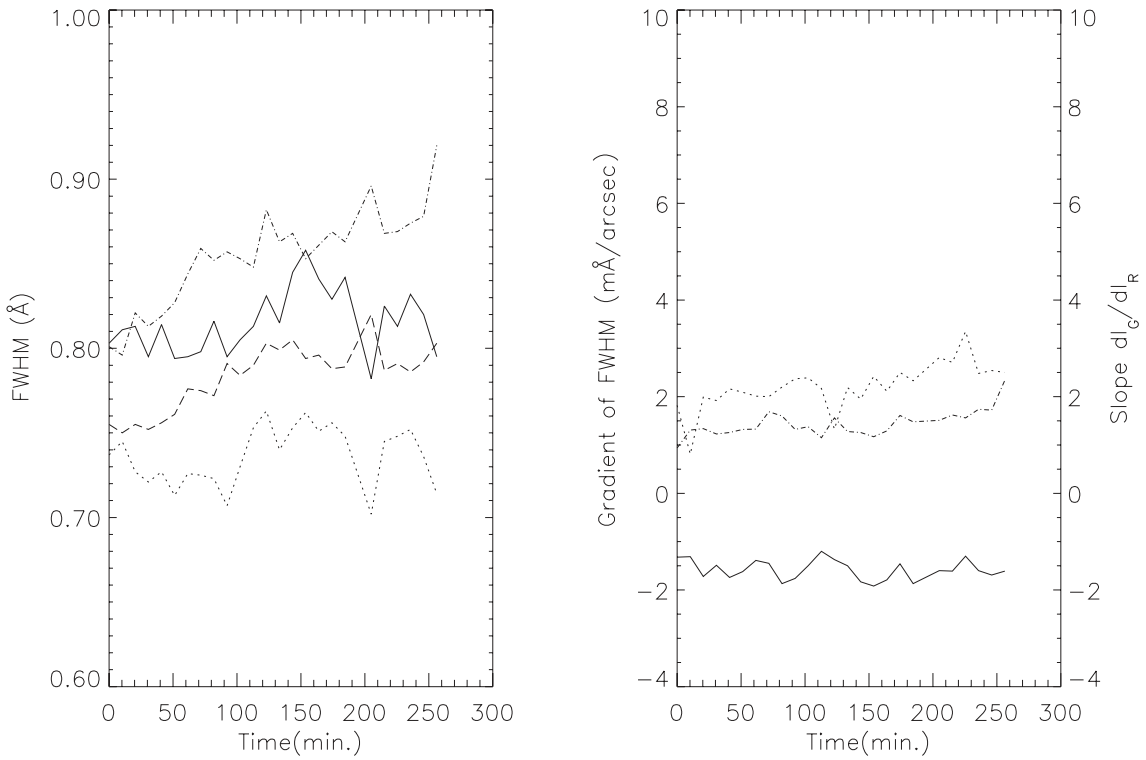

Fig. 7b. Same as figure 7a, but for the inner sub-structure of A.

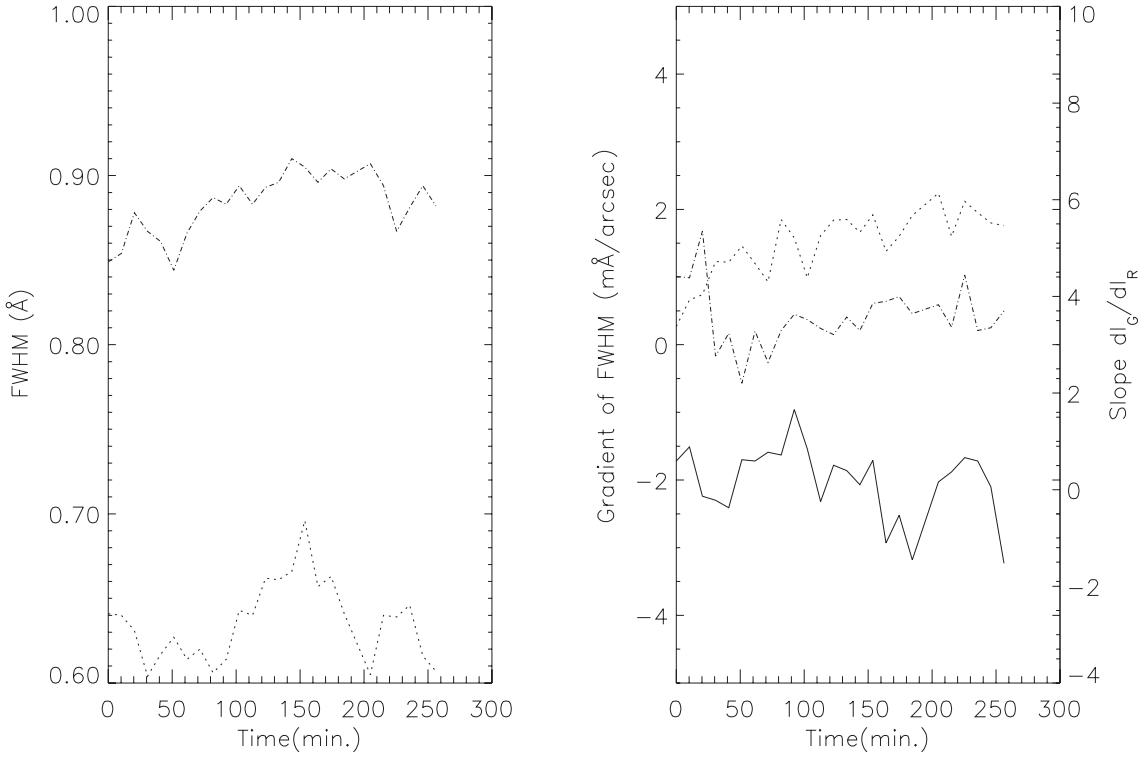

Fig. 7c. Same as figure 7a, but for only one location at 150″ of the top portion of the loop (C).

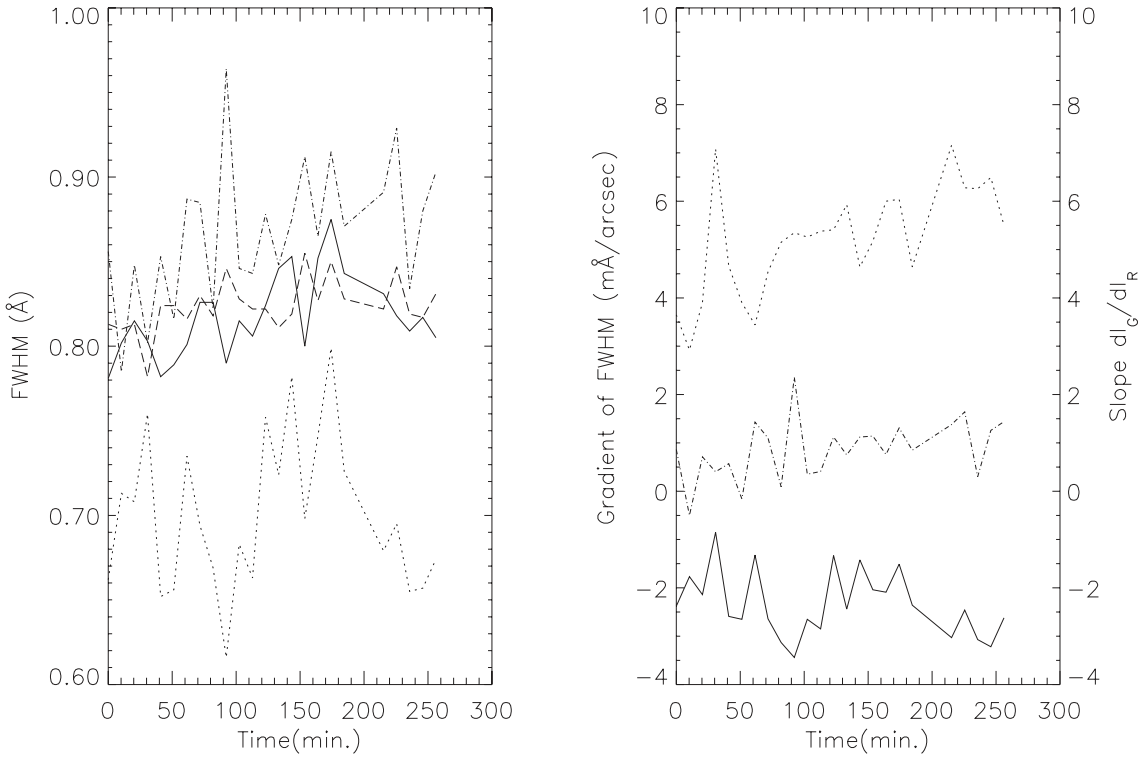

Fig. 7d. Same as figure 7a, but for the jet-like structure (D) in figure 2.

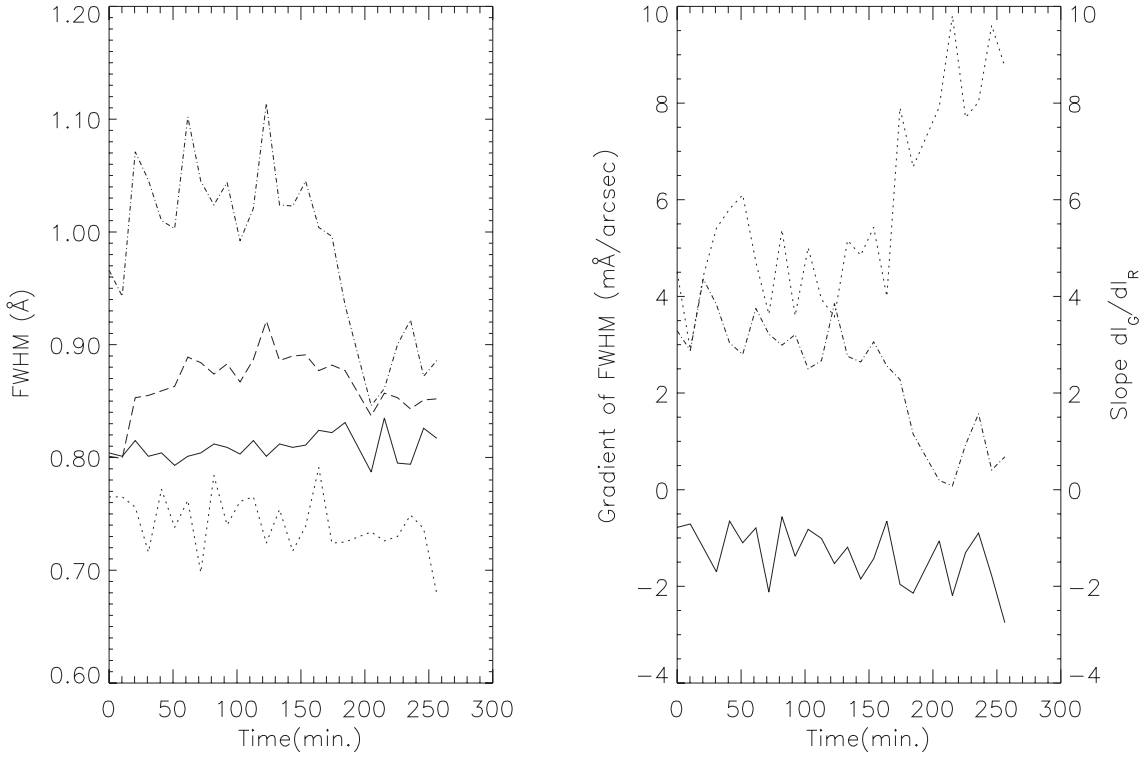

Fig. 7e. Same as figure 7a, but for the broad intense jet-like structure (F) in figure 2.

Table 3. Time-averaged values of FWHM (W) and gradients of FWHM (dW/dh) for the green and red lines in different coronal structures.

No.	$W_g(50'')$	$W_g(100'')$	$W_r(50'')$	$W_r(100'')$	dW_g/dh	dW_r/dh	Slope	Remark
	(mÅ)		(mÅ)		(mÅ arcsec^{-1})		$\delta I_g/\delta I_r$	
'Closed' structures								
1	816 ± 16	722 ± 27	807 ± 15	881 ± 30	-1.88 ± 0.38	1.45 ± 0.50	2.92 ± 0.13	Outer edge of 'A'
2	819 ± 21	731 ± 31	779 ± 17	845 ± 26	-1.77 ± 0.31	1.32 ± 0.32	1.74 ± 0.14	Inner sub-structure of 'A'
3	817 ± 25	734 ± 28	768 ± 17	822 ± 20	-1.68 ± 0.35	1.09 ± 0.24	2.56 ± 0.16	Inner sub-structure of 'A'
4	818 ± 18	723 ± 18	798 ± 18	834 ± 27	-1.90 ± 0.31	0.73 ± 0.44	7.45 ± 0.13	Inner edge of 'A'
5	814 ± 12	754 ± 19	788 ± 14	876 ± 25	-1.22 ± 0.26	1.77 ± 0.30	2.62 ± 0.11	Outer edge of 'B'
6	815 ± 19	736 ± 17	783 ± 19	854 ± 28	-1.58 ± 0.20	1.44 ± 0.27	2.21 ± 0.14	Inner sub-structure of 'B'
7	813 ± 17	727 ± 19	805 ± 24	853 ± 34	-1.73 ± 0.28	0.95 ± 0.34	3.14 ± 0.13	Inner sub-structure of 'B'
8	812 ± 14	727 ± 14	824 ± 11	839 ± 20	-1.70 ± 0.21	0.29 ± 0.26	4.63 ± 0.12	Inner edge of 'B'
9	$W_g(150'') = 636 \pm 23$		$W_r(150'') = 882 \pm 18$		-2.01 ± 0.53	0.41 ± 0.45	1.49 ± 0.15	Top of loop 'C'
'Open' structures								
10	820 ± 13	724 ± 40	859 ± 22	952 ± 41	-1.93 ± 0.68	1.86 ± 0.53	2.84 ± 0.12	Jet-like structure 'D'
11	817 ± 23	700 ± 45	824 ± 15	867 ± 40	-2.33 ± 0.67	0.86 ± 0.61	5.20 ± 0.15	Jet-like structure 'E'
12	809 ± 11	736 ± 21	851 ± 20	952 ± 75	-1.45 ± 0.50	2.02 ± 1.20	4.61 ± 0.10	Sub-structure of 'F'
13	809 ± 12	742 ± 26	865 ± 27	988 ± 73	-1.34 ± 0.58	2.43 ± 1.19	5.83 ± 0.11	Sub-structure of 'F'
14	795 ± 23	...	859 ± 20	...	-3.36 ± 0.75	0.67 ± 0.87	7.65 ± 0.15	Open structure 'G'

magnetic field is strong, the cool and the hot components may be separated; the contribution to the red-line emission comes from a relatively cooler plasma and to the green line from a relatively hotter plasma. As we move up along the coronal structure, the magnetic field spreads and weakens, and the mixing of hotter and cooler plasma may occur due to the existence of large thermal and non-thermal velocities. The mixed plasma at large heights may have an average temperature lower than that of the green-line plasma and higher than that of the red-line plasma at the bottom of the structure. This process can cause an increase in the width of the red line and a decrease in the green-line width with the height in the coronal structures. We should also point out that the decrease in the line width in the green line is not favorable for the interpretation that its non-thermal broadening is due to some kind of waves. The wave amplitude is expected to grow as the wave propagates higher

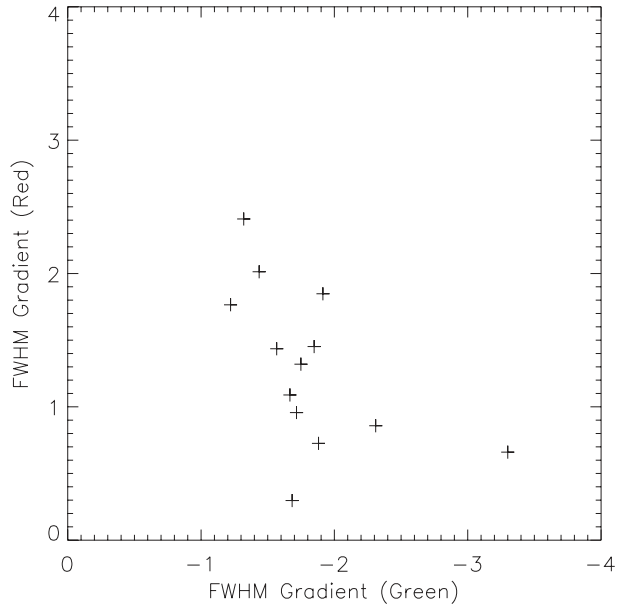

Fig. 8. Plot of FWHM gradients of the red line versus that of the green line.

toward the region of lower density.

One may also note that the width of the green line in both the open and closed structures is almost the same, whereas the width of the red line is larger in the open structures as compared to the closed loop-like structures. This means that the separation of the hot and the cool components is maintained along the open structure up to a height of 100″.

Alternatively, we may invoke a model proposed by Kuin and Martens (1982). In their picture, the corona is composed of loops that undergo cyclic non-equilibrium processes. When an excess energy is suddenly injected into a loop, the plasma at the footpoint is over-heated and expands into the loop. This process is the same as the so-called 'chromospheric evaporation' in flares, and the loop will attain a green-line temperature. As the loop cools, the plasma falls down along the magnetic fields, and we may find a cooler plasma toward the footpoints. The evacuated loop is now subjected to another heating episode, and the process will cyclically repeat. In this model, a coronal structure we observe is made of multiple (unresolved) loops at various phases of the cyclic process, and is inhomogeneous both in space and time. Recent observations of sporadic cooling events observed by TRACE (Schrijver 2001) may be a supporting evidence for this scenario.

From the observed variations of I_g/I_r ratios in general and the width variations of both the green and red lines with height above the limb, it appears that both the temperature and non-thermal velocity vary with height along the coronal structures. The height variation of the temperature derived from the intensity ratio, I_g/I_r, is rather complicated. Therefore, as a simplifying assumption we took an average value of $T = 1.5 \times 10^6$ K. We then found that the non-thermal velocity decreases when seen in the green line and increases when seen in the red line with height above the limb. In any case, the fractional change in temperature is marginal as compared to the dominant changes in non-thermal velocities. The values of the width gradient indicate that the variations in the temperature or turbulence, or both, are steeper in open coronal structures as compared to those in closed structures.

We should, however, be cautioned that our conclusions apply only up to a height of 200″ above the limb. The behavior of the emission lines in higher regions is still unknown. It is also possible that the properties of the coronal emission lines may change with the phase of the activity cycle. Data over longer periods and over a variety of structures are needed to investigate the properties of the coronal emission lines in more detail.

Part of this work was carried out while JS was a visiting scientist at the National Astronomical Observatory of Japan. He thanks A. V. Raveendran and H. Kurokawa for useful suggestions and J. S. Nathan for his help in handling software.

References

Bessey, R. J., & Liebenberg, D. H. 1984, Sol. Phys., 94, 239
Chandrasekhar, T., Desai, J. N., Ashok, N. M., & Pasachoff, J. M. 1991, Sol. Phys., 131, 25
Delone, A. B., & Makarova, E. A. 1969, Sol. Phys., 9, 116
Delone, A. B., & Makarova, E. A. 1975, Sol. Phys., 45, 157
Jarrett, A. H., & von Klüber, H. 1955, MNRAS, 115, 343
Jarrett, A. H., & von Klüber, H. 1961, MNRAS, 122, 223
Kuin, N. P. M., & Martens, P. C. H. 1982, A&A, 108, L1
Liebenberg, D. H., Bessey, R. J., & Watson, B. 1975, Sol. Phys., 44, 345
Livingston, W., & Harvey, J. 1982, Proc. Indian Natl. Sci. Acad., 48A, 18
Marshall, P. M., & Henderson, G. 1973, Sol. Phys., 33, 153
Raju, K. P. 1999, Sol. Phys., 185, 311
Raju, K. P., Desai, J. N., Chandrasekhar, T., & Ashok, N. M. 1993, MNRAS, 263, 789
Raju, K. P., Sakurai, T., Ichimoto, K., & Singh, J. 2000, ApJ, 543, 1044
Raju, P. K., & Singh, J. 1987, Sol. Phys., 110, 271
Schrijver, C. J. 2001, Sol. Phys., 198, 325
Singh, J. 1985, Sol. Phys., 95, 253
Singh, J., Bappu, M. K. V., & Saxena, A. K. 1982, J. Astrophys. Astron., 3, 249
Singh, J., Ichimoto, K., Imai, H., Sakurai, T., & Takeda, A. 1999, PASJ, 51, 269 (Paper I)